Chemistry Faculty Research and Publications   Chemistry, Department of

9-13-2012

Fe(II) Complexes That Mimic the Active Site Structure of Acetylacetone Dioxygenase: O₂ and NO Reactivity

Heoweon Park
Marquette University

Michael M. Bittner
Marquette University, michael.bittner@marquette.edu

Jacob Baus
Marquette University, jacob.baus@marquette.edu

Sergey Lindeman
Marquette University, sergey.lindeman@marquette.edu

Adam T. Fiedler
Marquette University, adam.fiedler@marquette.edu

Follow this and additional works at: https://epublications.marquette.edu/chem_fac

Part of the Chemistry Commons

Fe(II) Complexes That Mimic the Active Site Structure of Acetylacetone Dioxygenase: O₂ and NO Reactivity

Heaweon Park
Department of Chemistry, Marquette University, Milwaukee, Wisconsin
Michael M. Bittner
Department of Chemistry, Marquette University, Milwaukee, Wisconsin
Jacob S. Baus
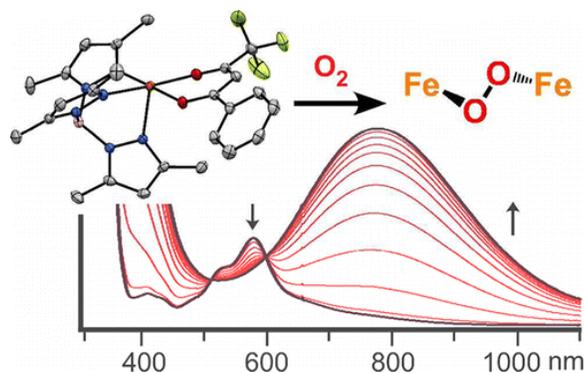Department of Chemistry, Marquette University, Milwaukee, Wisconsin
Sergey V. Lindeman
Department of Chemistry, Marquette University, Milwaukee, Wisconsin
Adam T. Fiedler
Department of Chemistry, Marquette University, Milwaukee, Wisconsin

Abstract

Acetylacetone dioxygenase (Dke1) is a bacterial enzyme that catalyzes the dioxygen-dependent degradation of β-dicarbonyl compounds. The Dke1 active site contains a nonheme monoiron(II) center facially ligated by three histidine residues (the 3His triad); coordination of the substrate in a bidentate manner provides a five-coordinate site for O_2 binding. Recently, we published the synthesis and characterization of a series of ferrous β-diketonato complexes that faithfully mimic the enzyme–substrate intermediate of Dke1 (Park, H.; Baus, J.S.; Lindeman, S.V.; Fiedler, A.T. *Inorg. Chem.* **2011**, *50*, 11978–11989). The 3His triad was modeled with three different facially coordinating N3 supporting ligands, and substituted β-diketonates (acac^X) with varying steric and electronic properties were employed. Here, we describe the reactivity of our Dke1 models toward O_2 and its surrogate nitric oxide (NO), and report the synthesis of three new Fe(II) complexes featuring the anions of dialkyl malonates. Exposure of [Fe(^{Me2}Tp)(acac^X)] complexes (where ^{R2}Tp = hydrotris(pyrazol-1-yl)borate with R-groups at the 3- and 5-positions of the pyrazole rings) to O_2 at −70 °C in toluene results in irreversible formation of green chromophores (λ_{max} ∼750 nm) that decay at temperatures above −60 °C. Spectroscopic and computational analyses suggest that these intermediates contain a diiron(III) unit bridged by a trans μ-1,2-peroxo ligand. The green chromophore is not observed with analogous complexes featuring ^{Ph2}Tp and ^{Ph}TIP ligands (where ^{Ph}TIP = tris(2-phenylimidazoly-4-yl)phosphine), since the steric bulk of the phenyl substituents prevents formation of dinuclear species. While these complexes are largely inert toward O_2, ^{Ph2}Tp-based complexes with dialkyl malonate anions exhibit dioxygenase activity and thus serve as functional Dke1 models. The Fe/acac^X complexes all react readily with NO to yield high-spin (S = 3/2) {FeNO}^{7} adducts that were characterized with crystallographic, spectroscopic, and computational methods. Collectively, the results presented here enhance our understanding of the chemical factors involved in the oxidation of aliphatic substrates by nonheme iron dioxygenases.

Synopsis

The reactivities of various Fe(II) β-diketonato complexes with O_2 and NO have been examined with spectroscopic, computational, and crystallographic methods. These complexes are models of the mononuclear nonheme Fe enzyme, acetylacetone dioxygenase (Dke1). The synthetic complexes react with O_2 to generate diiron(III) intermediates with trans μ-1,2-peroxo configurations, although dimerization is prevented by incorporation of sterically bulky substituents. Characterization of the Fe-NO adducts also sheds light on the electronic structure of the putative iron-superoxo intermediate in Dke1.

1 Introduction

The oxidative cleavage of carbon–carbon bonds by mononuclear nonheme iron dioxygenases is a crucial step in the microbial degradation of many organic pollutants.[1] Well-studied examples include the intradiol and extradiol catechol dioxygenases,[2] (homo)gentisate dioxygenases,[3] and (chloro)hydroquinone dioxygenases.[4] In 2003, Straganz and co-workers demonstrated that a strain of *Acinetobacter johnsonii* is able

to use acetylacetone—a toxic pollutant—as its sole source of carbon.(5) The initial step of this process is performed by the enzyme acetylacetone dioxygenase (also known as β-diketone dioxygenase, Dke1), which uses O_2 to convert acetylacetone to acetic acid and 2-oxopropanal.(5) Biochemical and crystallographic studies revealed that the Dke1 active site contains a monoiron(II) center facially ligated by three histidine (3His) residues, a deviation from the 2-His-1-carboxylate facial triad normally employed by nonheme iron dioxygenases.(6) Dke1 is capable of oxidizing β-diketones and β-ketoesters with a variety of substituents at the 1-, 3-, and 5-positions; in each case, the substrate coordinates to Fe as the deprotonated acac-type anion.(7) Initial mechanistic studies suggested that O_2 reacts with the bound acac ligand in a concerted two-electron process, resulting in a peroxidate intermediate without direct involvement of the Fe center.(8) However, in a subsequent computational study, Solomon and Straganz have set forth an alternative mechanism that involves formation of an Fe/O_2 adduct prior to substrate oxidation.(9)

Dke1 has attracted the interest of synthetic inorganic chemists because of the presence of the unusual 3His triad in the active site, as well as the enzyme's ability to catalyze aliphatic C–C bond cleavage. Interestingly, the first relevant model system was reported a decade before the discovery of Dke1. In 1993, Kitajima and co-workers generated the complex [Fe^{2+}(^{iPr2}Tp)(acac)(MeCN)] (where ^{R2}Tp = hydrotris(pyrazol-1-yl)borate with R-groups at the 3- and 5-positions of the pyrazole rings).(10) Exposure to O_2 in MeCN at room temperature eventually produced crystals of the triiron(III) complex [Fe_3(μ-O)(μ-OH)(μ-OAc)$_4$(^{iPr2}Tp)$_2$], where the bridging acetate ligands derive from the acac group of the ferrous precursor. Thus, this synthetic model exhibits Dke1-type reactivity, although generation of the acetate ligands may proceed via a different mechanism than the one employed by the enzyme. In 2008, Limberg and Siewert demonstrated that the related complex, [Fe^{2+}(^{Me2}Tp)(acac^{Phmal})] (acac^{Phmal} = anion of diethyl phenylmalonate), reacts with O_2 to give Dke1-type products with incorporation of oxygen atoms from O_2.(11) The activated diethyl malonate anion was used because the corresponding acac complex failed to exhibit oxidative cleavage. Significantly, the [Fe^{2+}(^{Me2}Tp)(acac^{Phmal})] system is catalytic in the presence of excess Li(acac^{Phmal}) and O_2 with a turnover frequency of 55 h^{-1}.

Recently, our group published the synthesis and characterization of three series of Dke1 models featuring Fe(II)/acac^X units (acac^X = substituted β-diketonates) bound to facially coordinating N3 supporting ligands (L_{N3}).(12) These complexes incorporated acac^X ligands with a range of steric and electronic properties. Following the labeling scheme employed in that paper (Scheme 1), the **1-acac^X** and **2-acac^X** complexes contain anionic ^{Me2}Tp and ^{Ph2}Tp donors, respectively. The **[3-acac^X]OTf** series utilizes the neutral tris(2-phenylimidazoly-4-yl)phosphine (^{Ph}TIP) ligand, which was shown by spectroscopic and computational analysis to faithfully reproduce the 3His coordination environment of the Dke1 active site. The present manuscript describes the reactivity of these complexes with O_2 and nitric oxide (NO) under a variety of conditions. To compare our results with those previously published by Siewert and Limberg, we have also generated three additional complexes that incorporate β-diester anions (i.e., acac^{OMe} and acac^{Phmal} in Scheme 1). Thus, we seek to expand upon previous discoveries that have demonstrated that synthetic Fe/acac^X complexes are capable of performing Dke1-type chemistry. In those earlier works, no attempt was made to observe reactive intermediates, and each involved only one Fe complex. In this study, using low-temperature techniques, we have identified and characterized intermediates arising from treatment of our Dke1 models with O_2 and NO. We have also systematically evaluated the role that solvent and ligand properties (both steric and electronic) play in modifying the O_2 reactivity of our complexes. Thus, we have developed a more complete and extensive picture of the nature of O_2 activation at nonheme Fe centers with relevance to Dke1.

Scheme 1

acac^X =

$acac^{OMe}$ $acac^{Phmal}$ acac $acac^{F_3}$ $acac^{PhF_3}$ $acac^{F_6}$
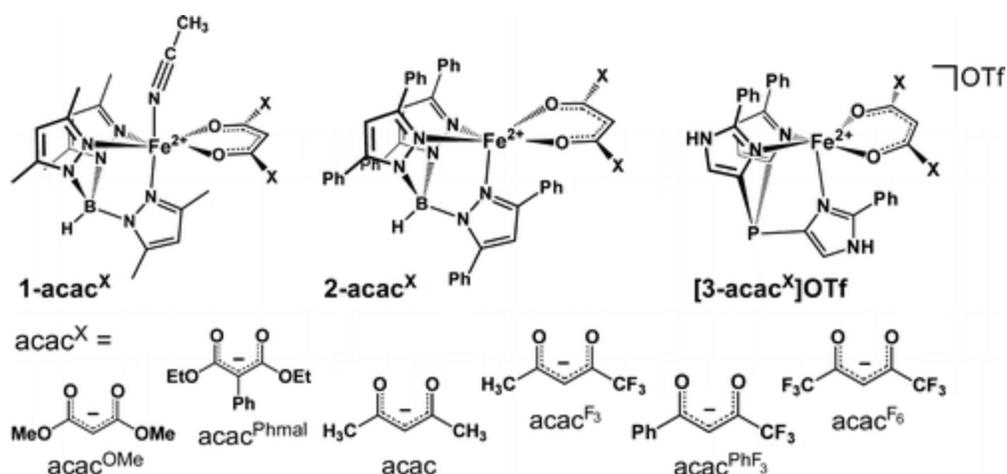
2 Experimental Section

Materials

Unless otherwise noted, all reagents and solvents were purchased from commercial sources and used as received. Acetonitrile, dichloromethane, and tetrahydrofuran were purified and dried using a Vacuum Atmospheres solvent purification system. The synthesis and handling of air-sensitive materials were performed under inert atmosphere using a Vacuum Atmospheres Omni-Lab glovebox equipped with a freezer set to −30 °C. Nitric oxide was purified by passage through an ascarite II column, followed by a cold trap at −78 °C to remove higher nitrogen oxide impurities. The L_{N3} supporting ligands K(^{Me2}Tp),(13) K(^{Ph2}Tp),(14) and ^{Ph}TIP(15) were prepared according to literature procedures. With the exceptions of **1-acac^{OMe}**, **2-acac^{OMe}**, and **2-acac^{Phmal}**, the synthesis and characterization of Fe(II) β-diketonato complexes in the **1-acac^X**, **2-acac^X**, and **[3-acac^X]OTf** series were reported in our earlier manuscript.(12)

Physical Methods

Elemental analyses were performed at Midwest Microlab, LLC in Indianapolis, IN. UV–vis absorption spectra were obtained with an Agilent 8453 diode array spectrometer equipped with a cryostat from Unisoku Scientific Instruments (Osaka, Japan) for low-temperature experiments. Infrared (IR) spectra were measured in solution using a Nicolet Magna-IR 560 spectrometer. ^{1}H and ^{19}F NMR spectra were collected at room temperature with a Varian 400 MHz spectrometer; ^{19}F NMR spectra were referenced using the benzotrifluoride peak at −63.7 ppm. Electron paramagnetic resonance (EPR) experiments were performed using a Bruker ELEXSYS E600 equipped with an ER4415DM cavity resonating at 9.63 GHz, an Oxford Instruments ITC503 temperature controller, and ESR-900 He flow cryostat. Mass spectra were recorded using an Agilent 6850 gas chromatography–mass spectrometer (GC-MS) with a HP-5 (5% phenylmethylpolysiloxane) column.

Synthesis of (^{Me2}Tp)Fe(acac^{OMe})

Following the procedure published by Siewert et al.,(11) dimethyl malonate (1.0 mmol) was deprotonated with lithium diisopropylamide (LDA; 1.1 mmol) in CH$_3$CN, followed by addition of FeCl$_2$ (1.0 mmol) and K(^{Me2}Tp) (1.0 mmol). The reaction mixture was stirred overnight, filtered, and the volume reduced under vacuum. X-ray quality crystals were obtained by storing this solution at −30 °C for several days. Anal. Calcd for C$_{20}$H$_{29}$BFeN$_6$O$_4$: C, 49.62; H, 6.04; N, 17.36. Found: C, 49.72; H, 5.89; N, 17.82. UV–vis [λ$_{max}$, nm (ε, M^{-1} cm^{-1}) in toluene]: 315 (sh). IR (KBr, cm^{-1}): 2952, 2930, 2526 [v(BH)], 1638 [v(CO)], 1542, 1498, 1451.

Synthesis of (^{Ph2}Tp)Fe(acac^{OMe})

Li(acac^{OMe}) was generated by treating dimethyl malonate (0.92 mmol) with LDA (1.0 mmol) in tetrahydrofuran (THF), followed by removal of the solvent to yield the salt as a white powder. FeCl$_2$ (0.92 mmol) and K(^{Ph2}Tp)

(0.92 mmol) were then combined with Li(acac^{OMe}) in 15 mL of 1:3 CH_2Cl_2/CH_3CN. The solution was stirred for 24 h, and the solvents were removed under vacuum. The white product was taken up in 5 mL of CH_2Cl_2 and filtered to remove insoluble salts. The resulting solution was layered with CH_3CN to yield colorless crystals suitable for XRD studies. Anal. Calcd for $C_{50}H_{41}BFeN_6O_4$: C, 70.11; H, 4.82; N, 9.81. Found: C, 70.02; H, 4.82; N, 9.85. UV–vis [λ_{max}, nm (ε, M^{-1} cm^{-1}) in toluene]: 330 (400). IR (KBr, cm^{-1}): 3061, 2950, 2616 [ν(BH)], 1632 [ν(CO)], 1503, 1460, 1304.

Synthesis of (^{Ph2}Tp)Fe(acac^{Phmal})

Diethyl phenylmalonate (Phmal) (0.712 mmol) was stirred with LDA (0.790 mmol) for 30 min in 5 mL of THF. Removal of the solvent yielded a white salt that was dissolved in a 3:2 mixture of MeCN/CH_2Cl_2. Addition of $FeCl_2$ (0.713 mmol) and K(^{Ph2}Tp) (0.712 mmol) resulted in a cloudy gray solution that was stirred overnight. The solvents were removed under vacuum to yield a pale green solid that was taken up in 5 mL of CH_2Cl_2 and layered with CH_3CN. After one day, light green crystals suitable for XRD were obtained. Anal. Calcd for $C_{58}H_{49}BFeN_6O_4$: C, 72.51; H, 5.14; N, 8.75. Found: C, 72.39; H, 5.11; N, 8.74. UV–vis [λ_{max}, nm (ε, M^{-1} cm^{-1}) in toluene]: 350 (1806). IR (neat, cm^{-1}): 3024, 2974, 2614 [ν(BH)], 1615 [ν(CO)], 1594, 1544, 1478, 1463, 1448, 1433, 1405, 1375, 1337, 1303.

Crystallographic Studies

Six novel complexes were characterized using X-ray crystallography: **1-acac^{OMe}**, **2-acac^{OMe}**, **2-acac^{Phmal}**, **1-acac^{PhF3}(NO)**, Fe(^{Ph2}Tp)$_2$, and [Fe$_3$(O)(OH)(OBz)$_4$(^{Me2}Tp)$_2$] (**5-acac^{PhF3}**). Details concerning the data collection and analysis are summarized in Table 1 and Supporting Information, Table S1. The XRD data were collected at 100 K with an Oxford Diffraction SuperNova kappa-diffractometer equipped with dual microfocus Cu/Mo X-ray sources, X-ray mirror optics, Atlas CCD detector, and a low-temperature Cryojet device. The data were processed with CrysAlisPro program package (Oxford Diffraction Ltd., 2010) typically using a numerical Gaussian absorption correction (based on the real shape of the crystal) followed by an empirical multiscan correction using the SCALE3 ABSPACK routine. The structures were solved using the SHELXS program and refined with the SHELXL program(16) within the Olex2 crystallographic package.(17) All computations were performed on an Intel PC computer with Windows 7 OS. Some structures contain disorder that was detected in difference Fourier syntheses of electron density and accounted for using capabilities of the SHELX package. In most cases, hydrogen atoms were localized in difference syntheses of electron density but were refined using appropriate geometric restrictions on the corresponding bond lengths and bond angles within a riding/rotating model (torsion angles of methyl hydrogens were optimized to better fit the residual electron density).

Table 1. Summary of X-ray Crystallographic Data Collection and Structure Refinement

	1-acac^{OMe}·MeCN	2-acac^{OMe}·1.5CH$_2$Cl$_2$	2-acac^{Phmal}·MeCN	1-acac^{PhF3}(NO)·MeCN·0.5CH$_2$Cl$_2$b
empirical formula	$C_{24}H_{35}BFeN_8O_4$	$C_{51.5}H_{44}BCl_3FeN_6O_4$	$C_{60}H_{52}BFeN_7O_4$	$C_{27.5}H_{32}BClF_3FeN_8O_3$
formula weight	566.26	983.94	1001.75	681.71
crystal system	orthorhombic	triclinic	monoclinic	monoclinic
space group	$P2_12_12_1$	$P\bar{1}$	$P2_1/c$	$P2_1/n$
a, Å	12.62432(13)	12.2090(3)	38.1369(8)	7.9307(2)
b, Å	16.70885(18)	13.0283(4)	13.5597(3)	19.6395(3)
c, Å	13.70225(15)	17.0877(5)	20.5303(4)	20.7317(5)
α, deg	90	95.921(3)	90	90
β, deg	90	103.201(3)	104.121(2)	91.126(2)
γ, deg	90	117.095(3)	90	90

V, Å^3	2890.32(5)	2287.5(1)	10295.9(4)	3228.4(1)
Z	4	2	8	4
D_{calc}, g/cm^3	1.301	1.429	1.293	1.366
λ, Å	0.7107	0.7107	1.5418	1.5418
μ, mm^{-1}	0.565	0.559	2.789	4.782
θ-range, deg	3 to 29	3 to 62	7 to 148	9 to 148
reflections collected	89285	49672	72082	28399
independent reflections	7745 [R_{int} = 0.0286]	13415 [R_{int} = 0.0278]	20374 [R_{int} = 0.0351]	6454 [R_{int} = 0.0393]
data/restraints/parameters	7745/0/354	13415/24/609	20374/0/1321	6454/0/445
GOF (on F^2)	1.057	1.031	1.040	1.122
$R1/wR2$ ($I > 2\sigma(I)$)a	0.0226/0.0608	0.0364/0.0861	0.0525/0.1393	0.0478/0.1268
$R1/wR2$ (all data)a	0.0251/0.0615	0.0463/0.0925	0.0570/0.1430	0.0546/0.1303

a$R1 = \sum ||F_o| - |F_c||/\sum |F_o|$; $wR2 = [\sum w(F_o^2 - F_c^2)^2/\sum w(F_o^2)^2]^{1/2}$.
bThe CH$_2$Cl$_2$ solvate in **1-acac^{PhF3}(NO)**·MeCN·0.5CH$_2$Cl$_2$ is only partially occupied.

Density Functional Theory (DFT) Calculations

DFT calculations were performed using the ORCA 2.8 software package developed by Dr. F. Neese.[18] Geometry optimizations employed the Becke–Perdew (BP86) functional[19] and Ahlrichs' valence triple-ζ basis set (TZV) for all atoms, in conjunction with the TZV/J auxiliary basis set.[20] Extra polarization functions were used on non-hydrogen atoms. The effect of toluene solvation on computational energies was accounted for using the conductor-like screening model (COSMO). The same basis set was used for time-dependent DFT (TD-DFT) calculations,[21] which computed absorption energies and intensities within the Tamm–Dancoff approximation.[22] In each case, at least 80 excited states were calculated. Finally, the gOpenMol program developed by Laaksonen[23] was used to generate isosurface plots of molecular orbitals.

3 Results and Analysis

3.A Synthesis, Solid State Structures, and Spectroscopic Features of Fe(II) Complexes

Following earlier procedures,[11, 12] the iron(II) complexes **1-acac^{OMe}**, **2-acac^{OMe}**, and **2-acac^{Phmal}** were prepared by reacting equimolar amounts of K(^{R2}Tp), FeCl$_2$, LDA, and dimethyl malonate or diethyl phenylmalonate. The resulting X-ray crystal structures are shown in Figure 1 and selected metric parameters are provided in Table 2. Like other members of the **1-acac^X** series,[12]**1-acac^{OMe}** features an octahedral Fe(II) center with a facially coordinating ^{Me2}Tp ligand, bidentate acac^{OMe} group, and MeCN. The average Fe–N$_{Tp}$ and Fe–O$_{acac}$ distances of 2.170 and 2.087 Å, respectively, resemble the values found for **1-acac** and are characteristic of high-spin six-coordinate (6C) Fe(II) complexes. The ^{Ph2}Tp complexes **2-acac^{OMe}** and **2-acac^{Phmal}** exhibit distorted 5C square-pyramidal geometries (τ = 0.03 and 0.39, respectively[24]) with a pyrazole ligand in the axial position. The lack of bound MeCN shortens the Fe–N$_{Tp}$ and Fe–O$_{acac}$ distances in **2-acac^{OMe}** and **2-acac^{Phmal}** relative to **1-acac^{OMe}** (Table 2). Because of steric interactions with the 3-Ph group of the axial pyrazole, the acac^{OMe} ligand is tilted out of the N1–Fe1–N3 plane by ∼30°.
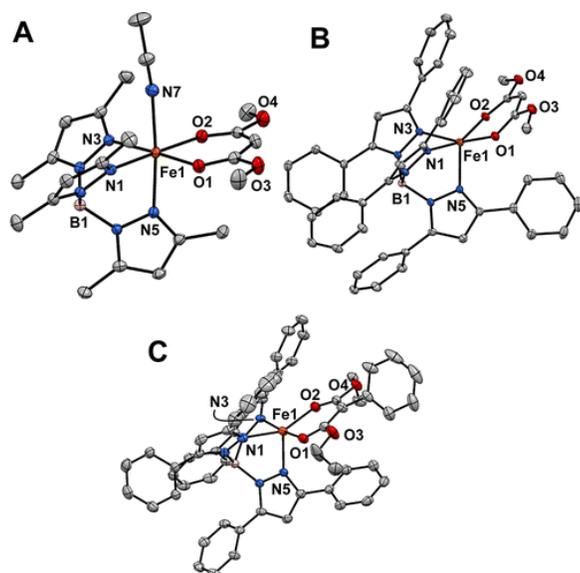
Figure 1. Thermal ellipsoid plots (50% probability) derived from **1-acac^{OMe}·MeCN (A)**, **2-acac^{OMe}·1.5CH₂Cl₂ (B)**, and **2-acac^{Phmal}·MeCN (C)**. Hydrogen atoms and noncoordinating solvent molecules have been omitted for clarity. Selected metric parameters are provided in Table 2.

Table 2. Selected Bond Distances (Å) and Bond Angles (deg) for 1-acac^{OMe}·MeCN, 2-acac^{OMe}·1.5CH₂Cl₂, and 2-acac^{Phmal}·MeCN

	1-acac^{OMe}·MeCN	2-acac^{OMe}·1.5CH$_2$Cl$_2$	2-acac^{Phmal}·MeCNa
Fe–O1	2.092(1)	2.042(1)	1.982(2)
Fe–O2	2.083(1)	2.046(1)	2.065(2)
Fe–N1	2.155(1)	2.151(1)	2.214(2)
Fe–N3	2.162(1)	2.154(1)	2.105(2)
Fe–N5	2.194(1)	2.129(1)	2.076(2)
Fe–N7	2.252(1)		
Fe–O$_{acac}$ (ave)	2.087	2.044	2.024
Fe–N$_{Tp}$ (ave)	2.170	2.144	2.132
O1–Fe–O2	86.70(3)	87.50(4)	86.34(6)
O1–Fe–N1	90.18(3)	92.16(4)	97.02(7)
O1–Fe–N3	177.00(3)	159.16(4)	147.45(7)
O1–Fe–N5	94.25(3)	108.31(4)	120.57(7)
O2–Fe–N1	176.86(4)	157.09(4)	170.87(7)
O2–Fe–N3	96.17(3)	88.54(4)	90.05(7)
O2–Fe–N5	92.16(4)	109.58(4)	95.66(7)
N1–Fe–N3	86.95(4)	83.68(4)	82.54(7)
N1–Fe–N5	88.45(4)	92.28(4)	89.95(7)
N3–Fe–N5	84.78(4)	92.29(4)	91.98(7)
τ-valueb		0.03	0.39

[a]The unit cell of **2-acac^{Phmal}·MeCN** contains two symmetrically independent complexes with nearly identical geometries. Only parameters of the first complex are shown.
[b]For a definition of the τ-value, see reference 24. A five-coordinate complex with ideal square-pyramidal geometry would have a τ-value of 0.0, while those with ideal trigonal bipyramidal geometry would have a value of 1.0.

Most Fe(^{R2}Tp)(acac^X) complexes are brightly colored because of the presence of Fe^{2+}→acac^X (C═O*) metal-to-ligand charge-transfer (MLCT) transitions in the visible region.(12) The acac^{OMe} and acac^{Phmal} complexes are colorless, however, as the corresponding MLCT bands appear in the UV-region, reflecting the electron-rich nature of the dialkyl malonate anions. The ^{1}H NMR spectra of these complexes exhibit broad, paramagnetically shifted peaks consistent with the presence of a high-spin Fe(II) center. For both **1-acac^{OMe}** and **2-acac^{OMe}**, resonances arising from the methyl groups of the acac^{OMe} moieties appear near 8 ppm in CD$_2$Cl$_2$. The remaining ^{R2}Tp-derived peaks largely follow the patterns previously described for complexes in the **1-acac^X** and **2-acac^X** series,(12, 25) and detailed assignments and T_1-relaxation values are provided in Supporting Information, Table S2.

Attempts to generate the analogous Fe(II)/β-diester complexes with the ^{Ph}TIP ligand (i.e., [**3-acac^{OMe}**]$^+$ or [**3-acac^{Phmal}**]$^+$) were not successful. This failure is perhaps due to the elevated basicities of the dialkyl malonate anions, which are incompatible with the unprotected H–N groups of the ^{Ph}TIP ligand.(26)

3.B Oxygenation of Fe(II) Complexes

As shown in Figure 2A, exposure of **1-acac^{OMe}** to O$_2$ at −70 °C in toluene gives rise to a dark *green intermediate* (**4-acac^{OMe}**) with an intense absorption band at 756 nm (ε = 2400 M^{-1} cm^{-1} per Fe). The oxygenation reaction is irreversible and the intermediate quickly decays at temperatures above −60 °C. Similar spectral changes are observed upon oxygenation of **1-acac** and **1-acac^{F3}** (Supporting Information, Figure S1) in toluene. Time-dependent absorption spectra of the reaction of **1-acac^{PhF3}** with O$_2$ (Figure 2B) display isosbestic points at 510 and 600 nm, indicative of clean conversion of **1-acac^{PhF3}**→**4-acac^{PhF3}** without the build-up of intermediates. While each green intermediate displays a prominent absorption band in the near-IR region, the energy and intensity of this band varies considerably within the series, suggesting that the acac^X ligand remains iron-bound and capable of modulating the electronic structures of **4-acac^X** (vide infra). Interestingly, **1-acac^{F6}** does not give rise to a green intermediate upon treatment with O$_2$, suggesting that the electron-poor acac^{F6} ligand deactivates the complex.
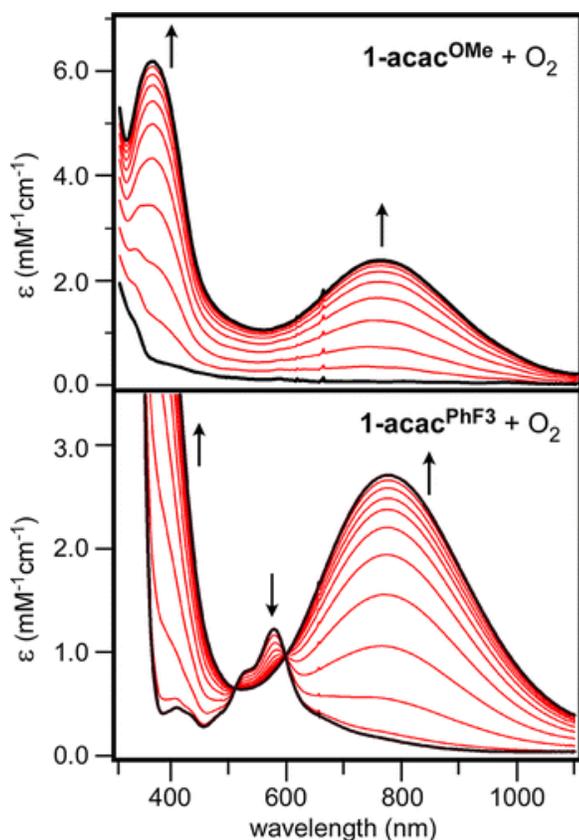
Figure 2. Time-dependent absorption spectra of the reaction of **1-acac^OMe** (top) and **1-acac^PhF3** (bottom) with O_2 at −70 °C in toluene. The molar absorptivities of the resulting **4-acac^X** intermediates are based on the initial concentrations of the **1-acac^X** precursors.

Formation of the green intermediates is hindered by the presence of coordinating solvents, such as MeCN and MeOH. As shown in Figure 3, oxygenation of **1-acac** in MeCN at −40 °C initially generates a broad absorption feature at 735 nm that likely corresponds to **4-acac**. This feature never reaches full intensity, however, because of a competing decay process that eventually yields a species (**5-acac**) with two intense, overlapping bands in the near-UV region. For other **1-acac^X** complexes (X = OMe, F_3, and PhF_3), the transient absorption band of the green intermediate is never observed during the reaction with O_2 in MeCN or MeOH; instead, these complexes directly convert to intermediates with UV–vis features similar to **5-acac** (Supporting Information, Figure S2). The **1-acac^X**→**5-acac^X** conversion occurs rapidly at −40 °C in the case of **1-acac^OMe**, whereas the process requires several days at room temperature for compounds with fluorinated acac^X ligands. Significantly, the addition of MeOH to toluene solutions of already-formed green intermediates results in immediate decay to the corresponding **5-acac^X** species, even at −70 °C. This behavior indicates that **4-acac^X** species are not stable in the presence of coordinating solvents.
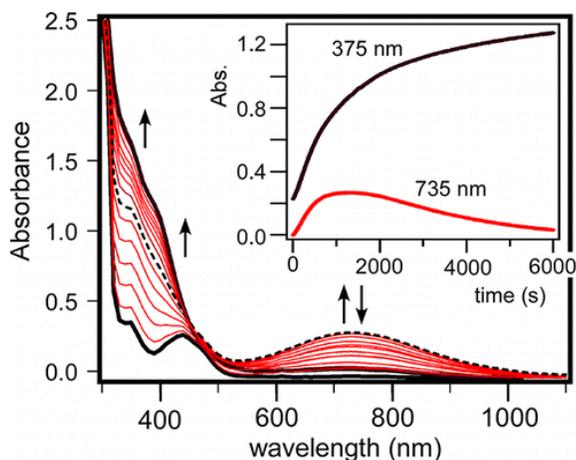
Figure 3. Time-dependent absorption spectra of the reaction of **1-acac** (0.4 mM) with O_2 at −40 °C in MeCN. Inset: Absorption intensity at 375 and 735 nm as a function of time.

The **5-acac^X** complexes are not simply the one-electron oxidized forms of **1-acac^X** (i.e., [Fe^{3+}(^{Me2}Tp)(acac^X)]$^+$), since treatment of **1-acac^X** complexes with ferrocenium salts yields chromophores with very different absorption features (Supporting Information, Figure S2). Instead, the spectral features resemble those reported by Kitajima et al. for the linear trinuclear ferric complex [Fe^{3+}$_3$(O)(OH)(OAc)$_4$(^{iPr2}Tp)$_2$] (**6**), which is generated upon exposure of [Fe^{2+}(^{iPr2}Tp)(acac)] to O_2 in MeCN (as noted in the Introduction).(10) In support of this assignment, the EPR spectra of **5-acac** and **5-acac^{PhF3}** display an intense feature at g = 4.3 and a weaker peak at g = 8.83 (Supporting Information, Figure S3), identical to the spectrum reported for **6**. In addition, crystals of **5-acac^{PhF3}** were obtained by allowing an aerobic solution of **1-acac^{PhF3}** in MeCN to stand for several weeks. XRD analysis revealed a triiron complex with C_s symmetry analogous to **6** (Supporting Information, Figure S4). The Fe centers in **5-acac^{PhF3}** are bridged by four benzoate ligands derived from the acac^{PhF3} ligand, as well as two μ-O(H) ligands. It is reasonable to assume that **5-acac** and **5-acac^{F3}** adopt similar structures. In the case of **5-acac^{OMe}**, however, the resulting methyl carbonate anion would decompose to CO_2 and methoxide, and therefore a trinuclear structure with bridging carboxylate ligands is unlikely. Attempts to crystallize **5-acac^{OMe}** have not succeeded to date. Regardless, our spectroscopic and crystallographic data prove that the reaction of [Fe(^{Me2}Tp)(acac^X)] complexes (where acac^X is a β-diketonate) with O_2 in coordinating solvents results in cleavage of the acac^X ligand, in agreement with previous studies by Kitajima(10) and Limberg(11) with related complexes.

Treatment of Fe(II) complexes in the **2-acac^X** and [**3-acac^X**]$^+$ series with O_2 failed to generate the corresponding green intermediates or triiron complexes under any conditions. These complexes react slowly, or not at all, with O_2 in both coordinating and noncoordinating solvents. For instance, the UV–vis absorption and ^{19}F NMR spectra of **2-acac^{F3}**, **2-acac^{PhF3}**, and [**3-acac^{F3}**]$^+$ in O_2-saturated toluene solutions exhibit no significant changes over the course of several days at room temperature. Only the β-diester complexes **2-acac^{OMe}** and **2-acac^{Phmal}** exhibit perceptible reactivity toward O_2. Exposure of these complexes to O_2 eventually yields colorless crystals that were shown by XRD to consist of Fe(^{Ph2}Tp)$_2$ (Supporting Information, Figure S5), suggesting that the acac ligands are degraded in the process.(27) Monitoring the O_2 reaction with ^{1}H NMR spectroscopy in toluene-d_8 revealed that the paramagnetically shifted peaks of **2-acac^{OMe}** and **2-acac^{Phmal}** slowly disappear, concomitant with the growth of peaks arising from methyl 2-oxoacetate and ethyl benzoylformate, respectively. The formation of ethyl benzoylformate was also verified by GC-MS. When the reaction with **2-acac^{Phmal}** was performed with ^{18}O-enriched dioxygen, GC-MS analysis indicated that one O-atom of ethyl benzoylformate is derived from O_2, proving that the observed products are due to dioxygenolytic cleavage of the ligand (the alkyl carbonate products that are also generated quickly decompose to CO_2 and the corresponding alkoxide). Thus, our ^{Ph2}Tp-based complexes are capable of performing Dke1-type chemistry on a reasonable time scale provided that the substrate ligand is sufficiently activated. The rates of the O_2 reactions in toluene were measured using UV–vis

absorption spectroscopy. **2-acac^{Phmal}** decays relatively quickly in the presence of O_2 (k_{O2} = 3.4 × 10^{-4} s^{-1}; Supporting Information, Figure S6), whereas **2-acac^{OMe}** requires more than a day for complete reaction (k_{O2} ~ 4 × 10^{-5} s^{-1}).

The observed reactivity trends of the Dke1 models cannot be rationalized on the basis of redox potentials. For instance, the Fe^{3+}/Fe^{2+} redox couple measured for the largely inert **2-acac** (−58 mV) is slightly more negative then the values for **1-acac^{F3}** (−34 mV vs Fc$^{+/0}$) and **1-acac^{PhF3}** (0 mV)(12) which react rapidly with O_2 to generate **4-acac^X** intermediates. In addition, cyclic voltammetric studies indicate that **2-acac^{Phmal}** is actually harder to oxidize than **2-acac** (Supporting Information, Figure S7); yet it is the former complex that carries out dioxygenolytic cleavage. Within the **2-acac^X** series, it appears that O_2 reactivity is primarily governed by the relative energies of acac^X π-electrons, not the Fe redox potentials. This conclusion is consistent with a prior study of Straganz that found a direct correlation between k_{cat} and the energy of the acac^X highest-occupied molecular orbital (HOMO).(8)

One might also ascribe the sluggish O_2 reactivity of the **2-acac^X** and [**3-acac^X**]$^+$ series to the increased steric bulk of the phenyl substituents, which appear to block access to the vacant coordination site in the X-ray crystal structures (Figure 1). However, this assumption is contradicted by our experiments with NO (vide infra). To understand the divergent O_2 chemistry of these complexes, it is necessary to identify the structure of the **4-acac^X** species formed upon reaction of some **1-acac^X** complexes with O_2.

3.C Spectroscopic and Computational Characterization of 4-acac^X Intermediates

Several pieces of evidence suggest that the green intermediates (**4-acac^X**) contain a diiron(III)-peroxo unit. First, the observed spectral features and the manner of preparation are very similar to those of the cis μ-1,2-peroxo bridged complex [Fe$_2$(O$_2$)(μ-O$_2$CR)$_2$(^{iPr2}Tp)$_2$] (**7**; R = Ph or CH$_2$Ph) first prepared by Kitajima and co-workers.(28) This complex is generated via the reaction of [Fe^{2+}(O$_2$CR)(^{iPr2}Tp)] with O_2 in toluene at −20 °C and features a band at 682 nm (ε = 1730 M^{-1} cm^{-1} per Fe) that arises from a peroxo→Fe(III) charge transfer transition.(29) Even more relevant to the current study is Kitajima's report that [Fe^{2+}(acac)(^{iPr2}Tp)] reacts with O_2 in toluene to give a green intermediate that is unstable even at −78 °C.(10) Although no spectroscopic characterization was performed, this species was presumed to be a μ-peroxo species. Second, we examined **4-acac** with magnetic circular dichroism (MCD) spectroscopy, which is sensitive to the ground-state spin of chromophores. As shown in Supporting Information, Figure S8, MCD spectra of **4-acac** fail to exhibit any temperature-dependent intensity in the 600–900 nm region. This result provides strong evidence in favor of an antiferromagnetically coupled diiron species (S_{total} = 0), while simultaneously ruling out a mononuclear Fe^{3+} or high-spin Fe^{2+} assignment for **4-acac**. Finally, EPR spectra of **4-acac^X** are featureless apart from a weak peak at g = 4.3 from the decomposition product (less than 10% of the Fe in the sample based on double integration of the signal(30)). Collectively, these results point to the formulation of **4-acac^X** as [Fe$_2$(μ-O$_2$)(acac^X)$_2$(^{Me}Tp)$_2$] intermediates. Unfortunately, further confirmation with resonance Raman spectroscopy has not been successful because of rapid photodecomposition of the green intermediates even at low laser power.

Possible structures for the **4-acac** intermediate were evaluated using DFT calculations. In the X-ray structure of **7**, the peroxo ligand adopts a cis μ-1,2-peroxo mode with two carboxylate ligands occupying μ-1,3 bridging positions between the two Fe^{3+} centers.(28b) An analogous structure is not possible for **4-acac**, since the acac ligands are not capable of bridging in a μ-1,5 fashion.(31) Given that each Fe center is likely coordinated to a single acac ligand, the most plausible structure of **4-acac** is a trans μ-1,2-peroxo diiron(III) complex with idealized C_{2h} symmetry, as shown in Figure 4. Geometry optimizations based on this orientation were carried out for the high-spin (HS), ferromagnetic state with S_{tot} = 5. While it is known from experiment that **4-acac** exhibits antiferromagnetic coupling, attempts to account for this fact with the broken-symmetry (BS) approach of Noodleman were not successful because of SCF convergence difficulties. Regardless, previous DFT studies of

transition metal dimers have demonstrated that HS and BS calculations generally provide similar geometries, and thus the HS models are sufficient for our purposes.(32)
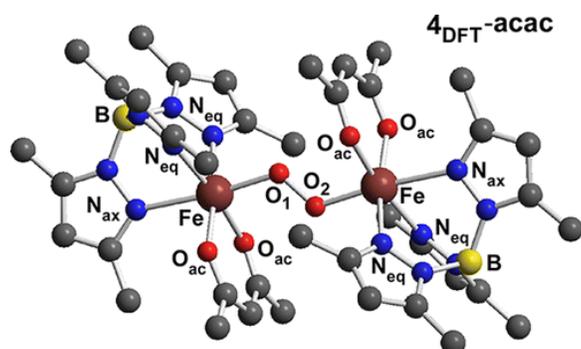

Figure 4. Model of **4-acac** derived from DFT geometry optimizations. The computed structure exhibits almost perfect C_{2h} symmetry. Computed bond distances (Å) and angles (deg): Fe–$O_{1(2)}$ 1.994, Fe–N_{eq} (ave) 2.173, Fe–N_{ax} 2.364, Fe–O_{ac} (ave) 2.037, O_1–O_2 1.389, Fe···Fe 4.882, Fe–O1–O1 122.8.

Significant metric parameters for the DFT-derived model of **4-acac** (**4$_{DFT}$-acac**) are provided in the caption of Figure 4. The computed O–O bond distance of 1.39 Å is characteristic of bridging peroxo ligands, and the Fe_2O_2 unit features Fe–O–O angles of 123° and a Fe–O–O–Fe dihedral angle near 180°. The trans μ-1,2 coordination of the peroxo moiety, combined with the fewer number of bridging ligands, results in a much larger Fe–Fe separation in **4$_{DFT}$-acac** (4.88 Å) than the crystal structure of **7** (4.00 Å).(28b) As a result, the Fe–O_{peroxo} bonds in **4$_{DFT}$-acac** are elongated by 0.09 Å relative to their counterparts in **7**.(33)

To validate the structure of **4$_{DFT}$-acac** on the basis of experimental data, electronic transition energies were calculated using time-dependent DFT (TD-DFT). The computed spectrum (Supporting Information, Figure S9) features a dominant band at 879 nm (11380 cm^{-1}) with an ε-value of 6300 M^{-1} cm^{-1} per Fe, in reasonable agreement with the experimentally observed feature at 740 nm (13510 cm^{-1}) with an ε-value of 3500 M^{-1} cm^{-1}. As expected, TD-DFT attributes this band to a peroxide(π_π*)→ Fe($3d_{xz}$) charge transfer transition. The intensity of this feature is enhanced by the planarity of the Fe_2O_2 unit in **4$_{DFT}$-acac**, which optimizes π-overlap between the π_π* and $3d_{xz}$ orbitals. For the sake of comparison, the TD-DFT methodology was also applied to a geometry-optimized model of complex **7**. The resulting calculation predicts a peroxide→ Fe CT transition at 788 nm (12690 cm^{-1}) with an intensity of 2200 M^{-1} cm^{-1} per Fe (experimentally, this band appears at 682 nm with ε = 1730 M^{-1} cm^{-1} per Fe(29)). It therefore appears that TD-DFT underestimates the transition energies and overestimates the intensities of CT features in diferric-peroxo complexes. Regardless, the computational results indicate that the principal peroxide→Fe CT transition of the putative trans μ-1,2 peroxo complex **4-acac** should be lower in energy and greater in intensity than the corresponding transition of the cis μ-1,2 peroxo complex **7**, which is fully consistent with our experimental observations.

Finally, computational methods were used to evaluate the stabilities of the diiron(III)-peroxo complexes relative to their 5C Fe^{2+} precursors and O_2. DFT-derived energies indicate that formation of **7**, via the reaction: 2Fe^{2+} + O_2 → Fe$_2$(μ-O_2), is more thermodynamically favorable than the formation of **4-acac** by nearly 14 kcal/mol.(34) This computational result is supported by numerous experimental observations that point to the greater stability of **7** relative to **4-acac**: (i) **7** is metastable at −20 °C,(28a) whereas **4-acac** decays rapidly at temperatures above −60 °C, (ii) X-ray quality crystals of **7** were obtained at low temperature,(28b) whereas crystallization of **4-acac** has proven futile to date, and (iii) **7** is more resistant to photodecomposition than **4-acac**. The enhanced stability of **7** relative to **4-acac** is likely due to the presence of the two bridging carboxylate ligands in the former.

On the basis of the spectroscopic and computational results presented here, we are confident that the **4-acac^X** chromophores correspond to diferric-peroxo complexes with trans μ-1,2-peroxo orientations, as shown in Figure 4 for **4-acac**.

3.D Reaction with Nitric Oxide

Nitric oxide has been frequently used to probe the ferrous states of nonheme Fe enzymes and related complexes. Each of our Dke1 models, regardless of its supporting ligand, rapidly reacts with NO to yield the corresponding {FeNO}^{7} species (according to the Enemark-Feltham notation(35)). As shown in Figure 5 for the representative reaction of **2-acac** with NO, formation of the greenish-brown Fe-NO adduct, **2-acac(NO)**, is evident in the appearance of two absorption bands near 440 and 620 nm that are characteristic of 6C {FeNO}^{7} species(36) (absorption spectra of all Fe-NO adducts generated as part of this study are shown in Supporting Information, Figures S10–S12). While iron-nitrosyl complexes with ^{R2}Tp supporting ligands have long lifetimes at room temperature (RT), the **3-acac(NO)** species is only moderately stable at −40 °C in MeCN. The nitrosyl complexes are uniformly high-spin (S = 3/2), displaying nearly axial EPR spectra with $g_x \approx g_y \approx 4.0$ and g_z = 2.0 (Figure 5, inset; see Supporting Information, Figures S12 and S13 for additional EPR data). In spectra measured in frozen CH$_2$Cl$_2$, poorly resolved superhyperfine splitting from the nitrogen ligands is evident in the g_x and g_y features. FTIR spectra of the NO adducts each revealed a prominent peak between 1720 and 1761 cm^{-1} arising from the stretching mode of the bound nitrosyl ligand. These v_{NO} frequencies are typical for high-spin, nonheme {FeNO}^{7} complexes with 6C geometries.(37)
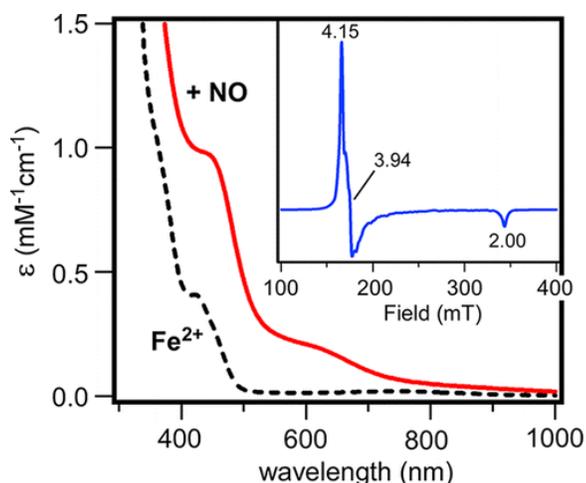

Figure 5. Absorption spectra of **2-acac** in CH$_2$Cl$_2$ at room temperature before and after addition of NO. Inset: X-band EPR spectrum of the Fe-NO adduct of **2-acac** in frozen CH$_2$Cl$_2$ ([Fe] = 1.5 mM). Instrumental parameters: frequency = 9.629 GHz; power = 2.0 mW; modulation = 12 G; temperature = 10 K.

X-ray quality crystals of **1-acac^{PhF3}(NO)** were obtained by slowly cooling a NO saturated solution of **1-acac^{PhF3}** in 1:1 MeCN:CH$_2$Cl$_2$. The crystal structure confirms the coordination of a NO ligand to the Fe center, providing a distorted octahedral geometry (Figure 6). Selected bond distances and angles for **1-acac^{PhF3}(NO)** are provided in Table 3. The FeNO unit is disordered over two positions in a 3:1 ratio with Fe1–N7–O3(A) angles of 147.7(3)° (major) and 139.4(6)° (minor).(38) As shown in Figure 6, the NO ligand in the major structural component is facing away from the acac^{PhF3} ligand, such that the projection of the NO bond vector bisects the N$_1$–Fe–N$_3$ angle (the N3–Fe1–N7–O3 dihedral angle is 41.5(5)°). In the minor structural component, the NO bond vector points in the opposite direction, bisecting the O1–Fe1–O2 angle of the acac^{PhF3} ligand; this orientation is similar to one likely adopted by O$_2$ in the Dke1 active site. Interestingly, the Fe1–N7 distance of 1.813(3) Å measured for **1-acac^{PhF3}(NO)** is significantly longer than the average Fe–N$_{NO}$ distance of ~1.73 Å found in comparable nonheme {FeNO}^{7} complexes, while the observed N–O distance of 1.148(4) Å is slightly shorter than the average value of ~1.16 Å.(37)
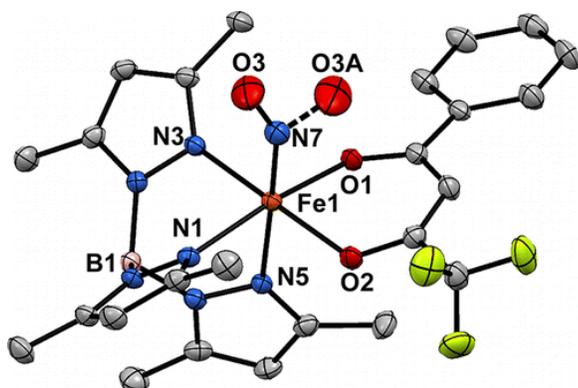
Figure 6. Thermal ellipsoid plots (50% probability) derived from the X-ray structure of **1-acac^{PhMe}(NO)·MeCN·0.5CH$_2$Cl$_2$**. Hydrogen atoms and noncoordinating solvent molecules have been omitted for clarity. The oxygen atom of the NO ligand (O3) is distorted over two positions in a 3:1 ratio. Selected metric parameters are provided in Table 3.

Table 3. Selected Bond Distances (Å) and Bond Angles (deg) for 1-acac^{PhF3}·MeCN and 1-acac^{PhF3}(NO)·MeCN·0.5CH$_2$Cl$_2$ Obtained via XRD Experiments[a]

	XRD		DFT
	1-acac^{PhF3}·MeCN	1-acac^{PhF3}(NO)·MeCN·0.5CH$_2$Cl$_2$	1-acac^{PhF3}(NO)
Fe–O1	2.064(1)	2.064(2)	2.104
Fe–O2	2.073(1)	2.069(2)	2.097
Fe–N1	2.144(1)	2.109(2)	2.136
Fe–N3	2.164(1)	2.112(2)	2.140
Fe–N5	2.170(1)	2.203(2)	2.219
Fe–N7	2.255(1)	1.813(3)	1.761
Fe–O$_{acac}$ (ave)	2.069	2.067	2.101
Fe–N$_{Tp}$ (ave)	2.158	2.141	2.165
N7–O3		1.148(4)	1.176
Fe–N7–O3		147.7(3)	143.4
O1–Fe–N3	175.48(5)	174.2(1)	172.9
O2–Fe–N1	177.83(5)	170.0(1)	173.4

[a]Metric parameters for the DFT-computed structure of **1-acac^{PhF3}(NO)** are also included.

The geometric changes arising from NO binding are evident in a comparison of the structure of **1-acac^{PhF3}(NO)** with its precursor **1-acac^{PhF3}** (Table 3). The trans influence of the nitrosyl ligand results in a lengthening of the Fe–N5 bond from 2.170(1) to 2.203(2) Å, and the Fe atom moves out of the N$_2$O$_2$ plane by 0.13 Å. In contrast, the equatorial Fe–N$_{Tp}$ bonds shorten by an average of 0.044 Å upon NO coordination, while the Fe–O$_{acac}$ distances remain the same within experimental error. The internal metric parameters of the acac^{PhF3} ligand are unchanged to within experimental error.

Using the X-ray structure as a starting point, the electronic structure of **1-acac^{PhF3}(NO)** was examined with spin-unrestricted DFT calculations employing the nonhybrid BP86 functional.(39) As shown in Table 3, the energy-minimized structure of **1-acac^{PhF3}(NO)** is reasonably consistent with the crystallographic data, exhibiting a rms deviation of 0.034 Å in the first-sphere Fe–N/O bond distances. However, DFT fails to reproduce the elongated Fe–N(O) bond observed for **1-acac^{PhF3}(NO)**, instead providing a more conventional value of 1.761 Å. DFT calculations employing hybrid functionals, such as B3LYP, resulted in Fe–N(O) distances that were too long

(>1.84 Å), while also overestimating the Fe–O$_{acac}$/N$_{Tp}$ distances to a greater degree than the BP86 structure. Thus, the BP model is likely the most accurate representation of the gas-phase structure of **1-acac^{PhF3}(NO)**.

The computed molecular orbital (MO) energy level diagram for **1-acac^{PhF3}(NO)** in the S = 3/2 ground state is shown in Figure 7. The frontier orbitals are primarily derived from the Fe 3d, NO(π^*), and acac^{PhF3} orbitals. The highest-occupied acac-based MO (acac HOMO) features a large lobe of electron density on the central carbon atom, corresponding to the acac "lone-pair", while the lowest-unoccupied acac-based MO (acac LUMO) has largely C=O* character. The two lowest-unoccupied spin-up (α) MOs are mainly composed of NO(π^*) character, indicating that the spin of the nitrosyl ligand is aligned opposite to the Fe spin (i.e., antiferromagnetic coupling). As illustrated by the contour plots shown in Figure 7, the Fe 3d(xz) and 3d(yz) orbitals interact strongly with the two spin-down (β) NO(π^*) orbitals. These MOs contain roughly equal amounts of Fe 3d and NO(π^*) character, and the same is true of their (unoccupied) antibonding counterparts. The high covalency of the Fe–NO bond makes it challenging to conclusively assign oxidation states for **1-acac^{PhF3}(NO)**, a difficulty encountered for nearly all iron nitrosyl complexes. Nonheme NO complexes with S = 3/2 have typically been described as high-spin Fe^{3+} centers (S = 5/2) coupled to NO$^-$ (S = 1).(36a) Consistent with this formulation, the energies of the Fe 3d(xy)- and 3d($x^2 - y^2$)-based MOs, which are nonbonding with respect to the axial ligands, decrease by approximately 0.9 eV upon conversion of **1-acac^{PhF3}→1-acac^{PhF3}(NO)**, indicating a significant increase in the Fe effective nuclear charge. The large amount of Fe 3d character (∼34%) in the spin-down HOMOs, however, suggests that the electron is only *partially* transferred from Fe to NO, resulting in an oxidation state between Fe^{3+} and Fe^{2+}.
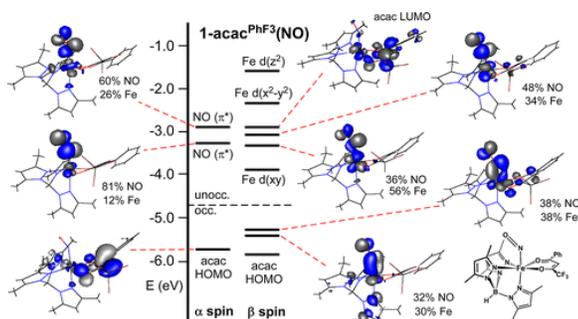

Figure 7. Molecular orbital energy-level diagram obtained from DFT calculations of **1-acac^{PhF3}(NO)**. MOs are labeled according to their principal contributor. DFT-generated isosurface plots and compositions of selected orbitals are also provided.

In many respects, **1-acac^{PhF3}(NO)** resembles an {FeNO}^{7} adduct recently synthesized and crystallographically characterized by Berto and Lehnert, namely, [Fe(NO)(Cl)(BMPA-Pr)] (**8**; where BMPA-Pr is *N*-propanoate-*N,N*-bis(2-pyridylmethyl)amine).(37b) Like **1-acac^{PhF3}(NO)**, complex **8** exhibits an axial S = 3/2 EPR sigand, along with a relatively long Fe–N(O) bond distance of 1.783 Å. DFT calculations of **8** revealed substantial mixing between the Fe 3d(xz/yz) and NO(π^*) orbitals in the β-manifold, similar to the bonding scheme described above for **1-acac^{PhF3}(NO)**. In these situations, Berto and Lehnert argue that the NO$^-$ ligand behaves as a strong π-donor, which lowers the effective nuclear charge of the Fe(III) center.

Complex **1-acac^{PhF3}(NO)** serves as an approximate model of the ferric–superoxo intermediate in the Dke1 mechanism. On the basis of DFT calculations, Diebold et al. have proposed that the superoxo group electrophilically attacks the acac HOMO to yield a peroxo bridge between Fe and the central C atom of the acac ligand.(9) This crucial step in the catalytic cycle would be facilitated by charge donation from the substrate HOMO to the Fe^{3+} center in the initial Fe/O$_2$ adduct, as likely occurs in the mechanism of extradiol catechol dioxygenases. Yet our calculations indicate that the acac^{PhF3} HOMO in **1-acac^{PhF3}(NO)** is essentially nonbonding with respect to the Fe-NO unit, and the amount of unpaired-spin density on the carbons atoms of the acac^{PhF3} ligand is negligible for both **1-acac^{PhF3}(NO)** and its ferrous precursor.

4 Discussion

This manuscript has described the reactivity of the Fe(II) β-diketonato complexes, $[Fe^{2+}(L_{N3})(acac^X)]$ ($L_{N3} = {}^{Me2}Tp$, ${}^{Ph2}Tp$, ${}^{Ph}TIP$), with O_2 and NO under various reaction conditions. On the basis of our observations, we propose the mechanistic framework shown in Scheme 2. With the exception of **1-acac^{F6}**, complexes in the **1-acac^X** series readily react with O_2 in toluene to produce dark green intermediates (**4-acac^X**) that are only stable at temperatures less than −60 °C. A combination of spectroscopic and computational results suggest that the **4-acac^X** intermediates consist of two $[Fe^{3+}({}^{Me2}Tp)(acac^X)]^+$ units linked by a trans μ-1,2-peroxide ligand (Figure 4). Given the generally accepted pattern of Fe/O_2 chemistry,(40) it is reasonable to assume that initial O_2 binding generates an iron(III)-superoxo intermediate (not observed) that quickly reacts with a second **1-acac^X** equivalent to form the diferric-peroxide intermediate, **4-acac^X**. In MeCN, reaction of some **1-acac^X** complexes with O_2 ultimately yields linear trinuclear complexes (**5-acac** and **5-acac^{PhF3}**) featuring four bridging carboxylates and two O(H) ligands (Supporting Information, Figure S4), as demonstrated previously by Kitajima and co-workers.(10) It is not certain if the formation of the triiron species proceeds via breakdown of the corresponding diiron(III)-peroxo intermediate or whether another mechanism is operative. While **4-acac** is indeed observed during the oxygenation of **1-acac** in MeCN (Figure 3), **4-acac^X** intermediates are not evident in the **1-acac^X→5-acac^X** conversions of the remaining complexes, although this result does not rule out transient formation of the green intermediates in these cases. Limberg has suggested that cleavage of the acac^X ligand in Kitajima's model (and in our systems, by extension) may be due to trace amounts of H_2O in MeCN, which could hydrolyze the acac^X ligand following oxidation of the Fe center.(11)

Scheme 2
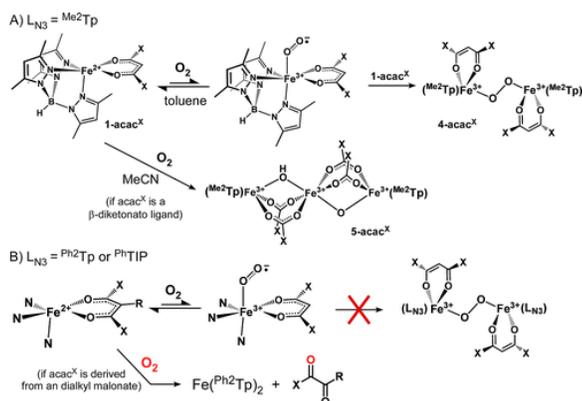
Compared to the **1-acac^X** series, Fe(II)-acac^X complexes with ${}^{Ph2}Tp$ or ${}^{Ph}TIP$ supporting ligands (**2-acac^X** and **[3-acac^X]$^+$**, respectively) exhibit dramatically diminished reactivity toward O_2. Complexes with β-diketonato ligands are stable in oxygenated solutions at room temperature for several hours or days, regardless of solvent. We initially assumed that this inert behavior was due to the steric bulk of the phenyl substituents, which might be expected to block O_2 coordination the Fe center. Yet this hypothesis is not consistent with the facile formation of $\{FeNO\}^7$ adducts upon exposure of the **2-acac^X** and **[3-acac^X]$^+$** complexes to NO, proving that formation of an Fe/O_2 species is sterically feasible for the ${}^{Ph2}Tp$- and ${}^{Ph}TIP$-based complexes. However, the size of the Ph groups likely prevents the second step in the pathway to **4-acac^X**, that is, formation of the diiron intermediate via reaction with a second Fe(II) complex (Scheme 2). Our DFT model of **4-acac** possesses a high degree of steric crowding even with relatively small methyl substituents on the pyrazole rings (Figure 4). The presence of phenyl rings at these positions would undoubtedly lead to severe steric clashes between opposing ${}^{Ph2}Tp$ (or ${}^{Ph}TIP$) ligands, thereby prohibiting formation of the analogous **4-acac^X** species.

The scenario illustrated in Scheme 2 requires the reaction equilibrium of the first step (i.e., O_2 binding) to lie far to the side of Fe(II) + O_2, since the putative iron(III)-superoxo adduct is never observed. Indeed, a number of

computational studies have demonstrated that the reversible transfer of one electron from a mononuclear nonheme Fe(II) center to O_2 is endergonic by approximately 5–10 kcal/mol.(9, 41) In our ^{Me2}Tp systems, the uphill nature of this initial step is overcome by the thermodynamic favorability of the second step, which "pulls" the entire process forward to **4-acac^X**. However, when this second step is hindered because of steric reasons, the ferrous complexes are rendered much less reactive toward O_2, as observed for the **2-acac^X** and **[3-acac^X]$^+$** series.

Obviously, the protein environment surrounding the Fe center in Dke1 prevents formation of a diiron-peroxo intermediate like **4-acac^X**. Instead, the enzymatic mechanism likely involves formation of a peroxy bridge between Fe and acac following initial formation of an iron(III)-superoxo species. One would therefore expect the ^{Ph2}Tp and ^{Ph}TIP supporting ligands, which prevent dimerization, to be ideal scaffolds for reproducing the catalytic activity of Dke1. Instead, only **2-acac^X** complexes with activated dialkyl malonate anions (**2-acac^{OMe}** and **2-acac^{Phmal}**) react with O_2 to give oxidized products. Since these complexes are not capable of forming diiron(III)-peroxo species like the ^{Me2}Tp-based complexes, the dioxygenolytic cleavage mechanism likely replicates the mechanism proposed by Diebold et al. for the enzyme.(9) However, even when dioxygenase activity is observed in our synthetic models, the rate of reaction is orders of magnitude slower than the rate of the enzyme with its natural substrate (k_{cat} = 6.5 s^{-1} for acetylacetone). Remarkably, Dke1 is capable of oxidizing unactivated substrates like acac^{F3} and acac^{PhF3} at measurable rates of 5.3 × 10^{-3} and 5.2 × 10^{-5} s^{-1};(8) by contrast, the corresponding synthetic complexes are stable in air for days.

The lackluster O_2 reactivity exhibited by complexes in the **2-acac^X** and **[3-acac^X]$^+$** series highlights the obstacles Dke1 must overcome to oxidize β-diketone substrates. As noted above, formation of the initial Fe/O_2 adduct has been shown to be endergonic in most nonheme Fe enzymes studied to date; therefore, enzymes rely on a favorable second-step to move the catalytic cycle forward. In the extradiol catechol dioxygenases, this process is facilitated by (partial or total) electron transfer from the bound catecholate substrate to Fe, resulting in a putative superoxo-Fe(II)-semiquinone intermediate. As demonstrated by Siegbahn, the radical character on the aromatic substrate lowers the barrier to peroxide formation.(41b) However, this strategy is not feasible in the case of Dke1, which involves oxidation of an aliphatic substrate. Our crystallographic and computational studies of **1-acac^X(NO)** adducts, reasonable models of the putative iron-superoxo intermediate in Dke1, failed to detect any significant radical character on the carbon backbone of the acac^X ligands. Thus, there appears to be an intrinsically large barrier to formation of the key alkylperoxo intermediate. The protein environment in Dke1 probably plays an important role in significantly lowering the barrier to O_2 reduction. This conclusion is consistent with computational and mutagenesis studies performed by Straganz and co-workers, who have demonstrated that changes in second-sphere residues (both hydrophilic and hydrophobic) significantly alter the rate of acetylacetone oxidation.(42) Nearby residues may function as acid/base catalysts, as is the case for ring-cleaving dioxygenases.(43) In a recent computational study, Christian et al. indicated that the barrier to alkylperoxo formation is lowered by simultaneous transfer of a proton to the proximal O-atom of the peroxo bridge.(44) While this study focused on the extradiol catechol dioxygenases, it is possible that a similar mechanism is operative in Dke1. The incorporation of these subtle second-sphere effects poses a challenge to the development of synthetic complexes capable of displaying Dke1-type reactivity.

Supporting Information

^{1}H NMR data for **1-acac^{OMe}** and **2-acac^{OMe}**, absorption spectra of **1-acac^X** complexes under various reaction conditions, crystallographic structures of **5-acac^{PhF3}** and Fe(^{Ph2}Tp)$_2$, MCD spectra of **4-acac**, metric parameters for DFT-optimized models and TD-DFT results, absorption and EPR spectra of Fe/NO adducts, and crystallographic data in CIF format. This material is available free of charge via the Internet at http://pubs.acs.org.

The authors declare no competing financial interest.

Terms & Conditions

Acknowledgment

References

1 (a) Costas, M.; Mehn, M. P.; Jensen, M. P.; Que, L., Jr. Chem. Rev. **2004**, 104, 939– 986 (b) Gibson, D. T.; Parales, R. E. Curr. Opin. Biotechnol. **2000**, 11, 236– 243 (c) Parales, R. E.; Haddock, J. D. Curr. Opin. Biotechnol. **2004**, 15, 374– 379

2 (a) Bugg, T. D. H.; Lin, G. Chem. Commun. **2001**, 11, 941– 953 (b) Bugg, T. D. H. Curr. Op. Chem. Biol. **2001**, 5, 550– 555 (c) Kovaleva, E. G.; Lipscomb, J. D. Nat. Chem. Biol. **2008**, 4, 186– 193

3 (a) Titus, G. P.; Mueller, H. A.; Burgner, J.; Córdoba, S. R. d.; Penalva, M. A.; Timm, D. E. Nat. Struct. Biol. **2000**, 7, 542– 546 (b) Vaillancourt, F. H.; Bolin, J. T.; Eltis, L. D. Crit. Rev. Biochem. Mol. Biol. **2006**, 41, 241– 267

4 (a) Machonkin, T. E.; Doerner, A. E. Biochemistry **2011**, 50, 8899– 8913 (b) Machonkin, T. E.; Holland, P. L.; Smith, K. N.; Liberman, J. S.; Dinescu, A.; Cundari, T. R.; Rocks, S. S. J. Biol. Inorg. Chem. **2010**, 15, 291– 301 (c) Yin, Y.; Zhou, N. Y. Curr. Microbiol. **2010**, 61, 471– 476

5 Straganz, G. D.; Glieder, A.; Brecker, L.; Ribbons, D. W.; Steiner, W. Biochem. J. **2003**, 369, 573– 581

6 (a) Leitgeb, S.; Nidetzky, B. Biochem. Soc. Trans. **2008**, 36, 1180– 1186 (b) Leitgeb, S.; Straganz, G. D.; Nidetzky, B. Biochem. J. **2009**, 418, 403– 411 (c) Diebold, A. R.; Neidig, M. L.; Moran, G. R.; Straganz, G. D.; Solomon, E. I. Biochemistry **2010**, 49, 6945– 6952

7 Straganz, G. D.; Hofer, H.; Steiner, W.; Nidetzky, B. J. Am. Chem. Soc. **2004**, 126, 12202– 12203

8 Straganz, G. D.; Nidetzky, B. J. Am. Chem. Soc. **2005**, 127, 12306– 12314

9 Diebold, A. R.; Straganz, G. D.; Solomon, E. I. J. Am. Chem. Soc. **2011**, 133, 15979– 15991

10 Kitajima, N.; Amagai, H.; Tamura, N.; Ito, M.; Morooka, Y.; Heerwegh, K.; Penicaud, A.; Mathur, R.; Reed, C. A.; Boyd, P. D. W. Inorg. Chem. **1993**, 32, 3583– 3584

11 Siewert, I.; Limberg, C. Angew. Chem., Int. Ed. **2008**, 47, 7953– 7956

12 Park, H.; Baus, J. S.; Lindeman, S. V.; Fiedler, A. T. Inorg. Chem. **2011**, 50, 11978– 11989

13 Malbosc, F.; Chauby, V.; Serra-Le Berre, C.; Etienne, M.; Daran, J. C.; Kalck, P. Eur. J. Inorg. Chem. **2001**, 2689– 2697

14 Kitajima, N.; Fujisawa, L.; Fujimoto, C.; Moro-oka, Y.; Hashimoto, S.; Kitagawa, T.; Toriumi, K.; Tatsumi, K.; Nakamura, A. J. Am. Chem. Soc. **1992**, 114, 1277– 1291

15 Kunz, P. C.; Klaeui, W. Collect. Czech. Chem. Commun. **2007**, 72, 492– 502

16 Sheldrick, G. M. Acta Crystallogr., Sect. A **2008**, 64, 112– 122

17 Dolomanov, O. V.; Bourhis, L. J.; Gildea, R. J.; Howard, J. A. K.; Puschmann, H. J. Appl. Crystallogr. **2009**, 42, 339– 341

18 Neese, F. ORCA - An ab initio, Density Functional and Semi-empirical Program Package, version 2.8; University of Bonn: Bonn, Germany, 2010.

19 (a) Becke, A. D. J. Chem. Phys. **1986**, 84, 4524– 4529 (b) Perdew, J. P. Phys. Rev. B **1986**, 33, 8822– 8824

20 (a) Schafer, A.; Horn, H.; Ahlrichs, R. J. Chem. Phys. **1992**, 97, 2571– 2577 (b) Schafer, A.; Huber, C.; Ahlrichs, R. J. Chem. Phys. **1994**, 100, 5829– 5835

21 (a) Stratmann, R. E.; Scuseria, G. E.; Frisch, M. J. J. Chem. Phys. **1998**, 109, 8218– 8224 (b) Casida, M. E.; Jamorski, C.; Casida, K. C.; Salahub, D. R. J. Chem. Phys. **1998**, 108, 4439– 4449 (c) Bauernschmitt, R.; Ahlrichs, R. Chem. Phys. Lett. **1996**, 256, 454– 464

22 (a) Hirata, S.; Head-Gordon, M. Chem. Phys. Lett. **1999**, 314, 291– 299 (b) Hirata, S.; Head-Gordon, M. Chem. Phys. Lett. **1999**, 302, 375– 382

23 Laaksonen, L. J. Mol. Graphics **1992**, 10, 33– &

24 Addison, A. W.; Rao, T. N.; Reedijk, J.; Vanrijn, J.; Verschoor, G. C. J. Chem. Soc., Dalton Trans. **1984**, 1349– 1356

25 Mehn, M. P.; Fujisawa, K.; Hegg, E. L.; Que, L., Jr. J. Am. Chem. Soc. **2003**, 125, 7828– 7842

26 The pK_a of dimethyl malonate is 16 in DMSO, while the corresponding value for imidazole is 18.6. For reference, the pK_a of acetylacetone is 13.6 in DMSO. Although the absolute pK_a values measured in DMSO and acetonitrile are expected to be quite different, the relative acidities are likely similar in the two solvents. Values were obtained from: Izutsu, K. Acid-Base Dissociation Constants in Dipolar Aprotic Solvents; Blackwell Scientific Publications: Oxford, U.K., 1990.

27 Limbergalso observed formation of the Fe(^{Me2}Tp)$_2$ complex upon reaction of their Dke1 model with O$_2$. See reference 11.

28 (a) Kitajima, N.; Tamura, N.; Amagai, H.; Fukui, H.; Moro-oka, Y.; Mizutani, Y.; Kitagawa, T.; Mathur, R.; Heerwegh, K.; Reed, C. A.; Randall, C. R.; Que, L., Jr.; Tatsumi, K. J. Am. Chem. Soc. **1994**, 116, 9071– 9085 (b) Kim, K.; Lippard, S. J. J. Am. Chem. Soc. **1996**, 118, 4914– 4915

29 Brunold, T. C.; Tamura, N.; Kitajima, M.; Moro-oka, Y.; Solomon, E. I. J. Am. Chem. Soc. **1998**, 120, 5674– 5690

30 Bou-Abdallah, F.; Chasteen, N. D. J. Biol. Inorg. Chem. **2008**, 13, 15– 24

31 β-diketonate ligands haven been shown to bridge metal centers in a μ-1,1 fashion. However, utilization of the μ-1,1 coordination mode in **4-acac** would result in coordinatively saturated Fe centers incapable of binding O$_2$.

32 (a) Sinnecker, S.; Neese, F.; Noodleman, L.; Lubitz, W. J. Am. Chem. Soc. **2004**, 126, 2613– 2622 (b) Binning, R. C.; Bacelo, D. E. J. Comput. Chem. **2008**, 29, 716– 723

33 This disparity between **4$_{DFT}$-acac** and **7** with respect to Fe-O$_{peroxo}$ distances is not due to deficiencies in the DFT methodologies, since our "control" calculation of **7** provided bond distances consistent with the reported crystal structure. In addition, steric crowding is only partially responsible for the elongated Fe-O$_{peroxo}$ bonds in **4$_{DFT}$-acac**, since replacement of the Tp methyl groups with hydrogen shortens the Fe-O$_{peroxo}$ bonds by a mere 0.02 Å.

34 The binding of O$_2$ is exothermic for both **7** (ΔH = −21.2 kcal/mol) and **4-acac** (ΔH = −9.3). As expected, the corresponding entropy terms are positive in both cases: +101 cal/K for **7** and +110 cal/K for **4-acac.**

35 Enemark, J. H.; Feltham, R. D. Coord. Chem. Rev. **1974**, 13, 339– 406

36 (a) Brown, C. A.; Pavlosky, M. A.; Westre, T. E.; Zhang, Y.; Hedman, B.; Hodgson, K. O.; Solomon, E. I. J. Am. Chem. Soc. **1995**, 117, 715– 732 (b) Chiou, Y. M.; Que, L. Inorg. Chem. **1995**, 34, 3270– 3278 (c) Hauser, C.; Glaser, T.; Bill, E.; Weyhermuller, T.; Wieghardt, K. J. Am. Chem. Soc. **2000**, 122, 4352– 4365 (d) Wasinger, E. C.; Davis, M. I.; Pau, M. Y. M.; Orville, A. M.; Zaleski, J. M.; Hedman, B.; Lipscomb, J. D.; Hodgson, K. O.; Solomon, E. I. Inorg. Chem. **2003**, 42, 365– 376 (e) Jackson, T. A.; Yikilmaz, E.; Miller, A. F.; Brunold, T. C. J. Am. Chem. Soc. **2003**, 125, 8348– 8363

37 (a) McCleverty, J. A. Chem. Rev. **2004**, 104, 403– 418 (b) Berto, T. C.; Hoffman, M. B.; Murata, Y.; Landenberger, K. B.; Alp, E. E.; Zhao, J. Y.; Lehnert, N. J. Am. Chem. Soc. **2011**, 133, 16714– 16717

38 The observed disorder in the FeNO unit is likely the result of crystal packing. In solution, the NO ligand is free to rotate, and the observed EPR parameters reflect an averaging of possible orientations.

39 In the DFT model of **1-acac^{PhF3}(NO**) described in the text, the NO ligand adopts the dominant orientation found in the X-ray structure. The alternative model based on the minor structure was also examined with DFT. The two models are essentially isoenergetic (ΔE = 0.8 kcal/mol, within the margin of error) and the electronic structures are nearly identical.

40 Mukherjee, A.; Cranswick, M. A.; Chakrabarti, M.; Paine, T. K.; Fujisawa, K.; Muenck, E.; Que, L., Jr. Inorg. Chem. **2010**, 49, 3618– 3628

41 (a) Davis, M. I.; Wasinger, E. C.; Decker, A.; Pau, M. Y. M.; Vaillancourt, F. H.; Bolin, J. T.; Eltis, L. D.; Hedman, B.; Hodgson, K. O.; Solomon, E. I. J. Am. Chem. Soc. **2003**, 125, 11214– 11227 (b) Bassan, A.; Borowski, T.; Siegbahn, P. E. M. Dalton Trans. **2004**, 3153– 3162

42 (a) Straganz, G. D.; Diebold, A. R.; Egger, S.; Nidetzky, B.; Solomon, E. I. Biochemistry **2010**, 49, 996– 1004 (b) Brkic, H.; Buongiorno, D.; Ramek, M.; Straganz, G.; Tomic, S. J. Biol. Inorg. Chem. **2012**, 17, 801– 815

43 Lipscomb, J. D. Curr. Opin. Struct. Biol. **2008**, 18, 644– 649

44 Christian, G. J.; Ye, S. F.; Neese, F. Chem. Sci. **2012**, 3, 1600– 1611